BIOCHEMISTRY
including biophysical chemistry & molecular biology

Article

pubs.acs.org/biochemistry

Conformational Dynamics in Human Neuroglobin: Effect of His64, Val68, and Cys120 on Ligand Migration

Luisana Astudillo,[†] Sophie Bernad,[‡] Valérie Derrien,[‡] Pierre Sebban,[‡,§] and Jaroslava Miksovska*[,†]

[†]Department of Chemistry and Biochemistry, Florida International University, Miami, Florida 33199, United States

[‡]Laboratoire de Chimie-Physique, Université Paris-Sud, CNRS UMR 8000, Bât. 350, 91405 Orsay Cedex, France

[§]University of Science and Technology of Hanoi/USTH, Building 2H, 18 Hoang Quoc Viet Street, Cau Giay District, Hanoi, Vietnam

ABSTRACT: Neuroglobin belongs to the family of hexacoordinate hemoglobins and has been implicated in the protection of neuronal tissue under hypoxic and ischemic conditions. Here we present transient absorption and photoacoustic calorimetry studies of CO photodissociation and bimolecular rebinding to neuroglobin focusing on the ligand migration process and the role of distal pocket residues (His64 and Val68) and two Cys residues (Cys55 and Cys120). Our results indicate that His64 has a minor impact on the migration of CO between the distal heme pocket and protein exterior, whereas the Val68 side chain regulates the transition of the photodissociated ligand between the distal pocket and internal hydrophobic cavities, which is evident from the increased geminate quantum yield in this mutated protein (Φ_{gem} = 0.32 for WT and His64Gln, and Φ_{gem} = 0.85 for Val68Phe). The interface between helix G and the A−B loop provides an escape pathway for the photodissociated ligand, which is evident from a decrease in the reaction enthalpy for the transition between the CO-bound hNgb and five-coordinate hNgb in the Cys120Ser mutant (ΔH = −3 ± 4 kcal mol^{-1}) compared to that of the WT protein (ΔH = 20 ± 4 kcal mol^{-1}). The extensive electrostatic/hydrogen binding network that includes heme propionate groups, Lys67, His64, and Tyr44 not only restricts the heme binding but also modulates the energetics of binding of CO to the five-coordinate hNgb as substitution of His64 with Gln leads to an endothermic association of CO with the five-coordinate hNgb (ΔH = 6 ± 3 kcal mol^{-1}).

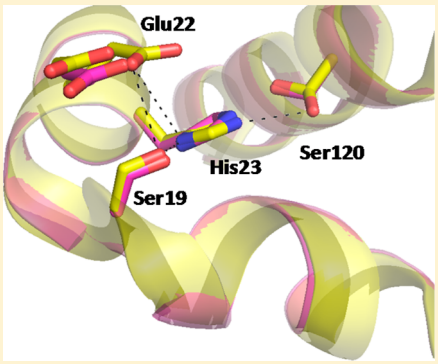

Neuroglobin (Ngb) is a small heme-containing globin, composed of 151 amino acid residues, that is mainly expressed in the brain and retina of vertebrates.[1] Overexpression of Ngb was observed in rat neurons exposed to hypoxia and focal ischemia conditions.[2] An increased level of Ngb expression also promotes neuron survival after ischemic insults.[2,3] The molecular basis of the neuroprotective function of Ngb remains unclear, but several plausible mechanisms have been proposed, including oxygen storage,[2,4] oxygen/redox sensing,[5] decomposition of reactive oxygen species,[6,7] and inhibition of apoptosis.[8,9] In addition, Wakasugi et al.[5] reported that ferric Ngb binds to the GDP-bound form of the α-subunit of the heterotrimeric G protein acting as a guanine nucleotide dissociation inhibitor and the interactions between hNgb and the G protein may promote cell survival.[10] Alternatively, Brittain et al.[11] showed that *in vivo* Ngb inhibits apoptosis through the binding to cytochrome *c* and preventing procaspase 9 activation.

The three-dimensional structure of Ngb (Figure 1) can be nearly superimposed with that of myoglobin (Mb) despite the low degree of sequence homology (~30%).[12−15] Ngb displays the classical 3-over-3 α-helical globin fold with the heme iron being hexacoordinated in both ferric and ferrous forms with His96 and His64 serving as the endogenous ligands. The distal His64 can be readily replaced by diatomic ligands, including O_2, CO, and NO that reversibly bind to the heme iron.[4,6,16] The competition between the distal histidine and exogenous ligand leads to biphasic ligand binding kinetics, with His64 dissociation being the rate-limiting step.[4]

In addition to the hexacoordination of the heme iron, other structural factors alter interactions of Ngb with diatomic ligands. An overlay of the crystal structure of the ligand free and CO-bound mouse Ngb (mNgb) reveals that the association of the ligand with the heme iron triggers reorganization of the heme distal pocket that is unique among vertebrate globins, including sliding of the heme group deeper into the distal cavity, reorganization of helix F, and alteration of C−D and E−F loop mobility.[13] However, such heme displacement may be species-dependent as shown in computational studies.[17,18]

An intriguing structural feature of human Ngb (hNgb) is the presence of an internal disulfide bond between Cys46 and Cys55 that is missing in rat Ngb (rNgb) and mouse Ngb (mNgb). Hamdane et al.[19] have demonstrated that the reduction of the internal disulfide bond or replacement of one of the Cys residues decreases the rate of dissociation of His64 from heme iron by a factor of 10, resulting in a

Received: July 27, 2012
Revised: November 20, 2012
Published: November 24, 2012

   dx.doi.org/10.1021/bi301016u | *Biochemistry* 2012, 51, 9984−9994

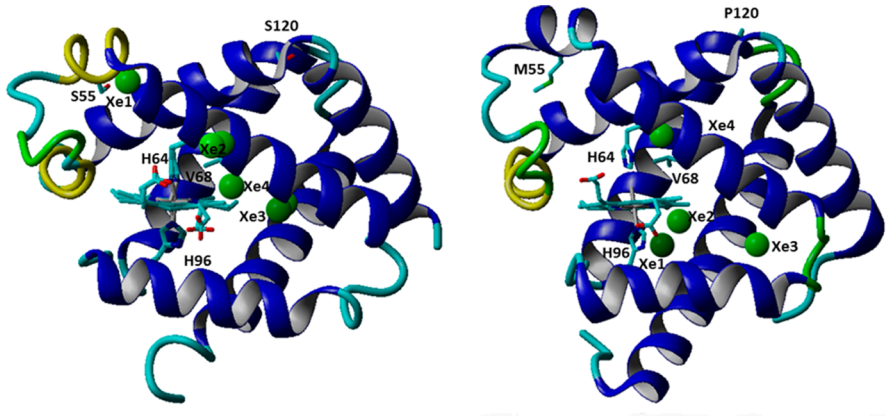

Figure 1. Ribbon representation of ferric mNgb (left, PDB entry 3GK9) and sperm whale Mb (right, PDB entry 1J52) depicting the position of the heme group, proximal His96, and distal His64, Val68, Ser120, and Ser 55 in Ngb and analogous residues in Mb. Xe cavities are depicted as green spheres.

diminishing of the affinity of hNgb for O_2. On the basis of these results, it was proposed that the interaction between Ngb and O_2 may be coupled to the intracellular redox state through the rupture and/or formation of the internal disulfide bond.[19] Recently, we have shown that the structural volume change associated with photodissociation of CO from rNgb or hNgb lacking the disulfide bond is approximately 3 times larger than that measured for wild-type hNgb, suggesting that the internal disulfide bond also impacts the structural dynamics associated with binding of CO to the five-coordinate Fe^{2+}Ngb.[20] The molecular mechanism of how structural changes in the C−D loop are relayed to the heme distal pocket remains unclear, although Phe28 was recently identified as a key residue in the communication between the C−D loop and the heme pocket.[21]

The crystal structures of Fe^{2+}mNgb and COmNgb also show an extensive network of hydrophobic cavities that partially overlay with the Xe cavities identified in Mb.[22] The volume and the spatial organization of this hydrophobic network depend on the heme iron coordination. Furthermore, the transition from the six-coordinate CO-bound Fe^{2+}mNgb to six-coordinate bishistidyl Fe^{2+}mNgb is associated with an increase in the cavity volume and opening of a direct pathway between the heme binding pocket and surrounding solvent.[13] The physiological role of the hydrophobic cavities remains unclear; however, they may provide ligand migration pathways and/or temporary storage for diatomic gases. Indeed, experimental and theoretical studies have shown that ligand exchange between the heme binding pocket and surrounding solvent is significantly faster in Ngb than in Mb.[20,23,24] Anselmi et al.[24] have proposed that the photoreleased ligand escapes from the distal pocket through two hydrophobic cavities that are analogous to the Xe_2 and Xe_4 sites in Mb and with an estimated time for the escape of CO from the protein matrix of 25 ns. This is consistent with the results of previous transient absorption studies that report a rate constant for the release of the ligand from the protein matrix of 1.4×10^8 s^{-1}, which is ~20 times faster than in Fe^{2+}Mb ($k = 5.3 \times 10^6$ s^{-1}), and with results of photoacoustic calorimetry (PAC) studies indicating that the CO escapes into the surrounding solvent within 50 ns subsequent to photodissociation of the Fe−CO bond.[20]

To provide detailed insight into the mechanism of interaction of diatomic ligands with Ngb and the role of conserved distal pocket residues His64 and Val68 in the binding of the ligand to hNgb, we have used PAC and transient absorption (TA) spectroscopy to characterize the time-resolved thermodynamics and kinetics of CO photorelease and thermal binding to Ngb. Moreover, the impact of the two conserved cysteine residues, Cys120 and Cys55, on ligand binding properties is examined. The Cys120 residue is located at the interface of helix G and the loop between helices A and B, whereas Cys55 is found within the flexible C−D loop and forms an internal disulfide bond with Cys46 in hNgb.

MATERIALS AND METHODS

Fe^{3+}tetrakis(4-sulfonatophenyl)porphine [Fe(III)4SP] was purchased from Frontier Scientific Inc. Dithiothreitol (DTT) and 5-aminolevulenic acid were purchased from Sigma-Aldrich. All other reagents were purchased from Fisher Scientific and used as received.

Protein Preparation. The coding sequence of hNgb with a six-His tag at the N-terminus was cloned into a pET15b expression vector. The DNA sequence of the recombinant plasmid product was confirmed through DNA sequencing. The QuickChange site-directed mutagenesis method (Stratagene) was employed to introduce mutations into the Ngb coding sequence. The expression vectors were then transformed into *Escherichia coli* strain BL21. Cells were then grown in 50 mL of Luria-Bertani medium supplemented with 100 mg L^{-1} ampicillin for 8 h at 37 °C. Subsequently, 10 mL of culture was transferred into 1 L of Terrific Broth medium supplemented with 100 mg L^{-1} ampicillin and 170 mg L^{-1} 5-aminolevulenic acid. Cells were incubated at 37 °C and 200 rpm, until A_{600} reached 1.1. The culture was induced by addition of isopropyl β-D-1-thiogalactopyranoside to a final concentration of 0.4 mM. Cells were then incubated overnight at 30 °C, collected by centrifugation for 10 min at 2700*g* and 4 °C (Allegra 64R, Beckman Coulter), and homogenized in 50 mM Tris buffer and 5 mM DTT (pH 8.0). The suspension was sonicated with a sonic dismembrator (model 100, Fisher Scientific) and centrifuged at 24000*g* to remove membrane debris. The supernatant was filtered through a 0.2 μm membrane and loaded into a Ni-NTA column (Qiagen) that was previously equilibrated with 10 mM Tris buffer (pH 8.0). The column was then washed with 10 mM Tris buffer (pH 8.0) containing increasing concentrations of imidazole (5, 10, 15, and 20 mM) until the absorbance at 280 nm was <0.03. Ngb was eluted with 10 mM Tris buffer (pH 8.0) containing 40 mM imidazole. Fractions with an A_{Soret}/A_{280} ratio of >3.0 were

dx.doi.org/10.1021/bi301016u | *Biochemistry* 2012, 51, 9984−9994

collected, concentrated using Amicon Millipore concentrators, and dialyzed overnight against 50 mM Tris buffer (pH 7.0). The purity of the protein was assessed using sodium dodecyl sulfate electrophoresis.

Preparation of Samples for TA and PAC Measurements. Ngb was dissolved in 50 mM Tris buffer (pH 7.0). CO-bound ferrous Ngb samples were obtained by placing samples into 0.5 cm × 1.0 cm or 0.2 cm × 1.0 cm quartz cuvettes sealed with a septum cap. Samples were then purged with Ar for approximately 10 min and reduced with a few microliters of freshly prepared 1 mM sodium dithionate. Subsequently, the sample was purged with CO, and the formation of the CO-bound Ngb adduct was verified by monitoring the UV−visible absorption spectra (single-beam spectrophotometer, Cary 50, Varian). The Ngb concentration was calculated using an ε_{532} of 10.7 mM^{-1} cm^{-1} for metNgb.[25]

Transient Absorption Spectroscopy. The kinetics of rebinding of CO to Ngb on a micro- to millisecond time scale were observed using a home-built transient absorption instrument described previously.[26] The sample in an optical cell was placed in a temperature-controlled cell holder (Quantum Northwest), and the probe beam (output from a 200 W Xe arc lamp, Newport) was focused on the center of the cell. The emerging light was passed through a monochromator (Jobin Yvon), and the change in absorbance was detected at 436 nm using a photodiode (model 818-BB-22, Newport). The signal was then amplified (C6438-01, Hamamatsu) and stored in a 400 MHz digitizer (Wave Surfer 42Xs, LeCroy). The photodissociation of CO was triggered using the 532 nm output of a Nd:YAG laser (50 μJ, 7 ns pulse width, Minilite II, Continuum). Submicrosecond CO rebinding kinetics were probed using a broadband pump−probe subnanosecond transient absorption spectrometer (EOS, Ultrafast Systems, LLC, Sarasota, FL). CO photodissociation was triggered using a Ti-sapphire laser (~35 fs pulse, Legend Elite, Coherent) with an output of 400 nm. The change in absorbance was detected through a fiber optic cable coupled to a multichannel spectrometer with CMOS sensors (1.5 nm resolution). TA traces were analyzed using Origin, version 8.0 (OriginLab Corp.).

Photoacoustic Calorimetry. The PAC instrumental setup has been described previously.[27,28] Samples were placed in a temperature-controlled cuvette holder (Quantum Northwest). The 532 nm output from a Nd:YAG laser (50 μJ, 7 ns pulse width, Minilite II, Continuum) was passed through a narrow slit (100 μm) placed in front of the optical cell. A 1 MHz acoustic detector (model RV103, Panametrics) was attached to the side of the cell using a thin layer of honey. The acoustic signal was amplified using an ultrasonic amplifier (model 5662, Parametrics) and stored in a 400 MHz digitizer (Wave Surfer 42Xs, Le Croy). PAC traces were analyzed using Origin, version 8.0 (OriginLab Corp.).

Data Analysis. The data analysis used for PAC has been previously reviewed.[27,28] The amplitude of the acoustic signal, S, taken as the difference between the first maximum and minimum of the acoustic wave, can be expressed as the sum of two contributions according to eq 1:

$$S = KE_a\left(Q\frac{\beta}{C_p\rho} + \Delta V_{nonthermal}\right) \quad (1)$$

where the $Q[\beta/(C_p\rho)]$ term corresponds to the thermal volume change ($\Delta V_{thermal}$) and $\Delta V_{nonthermal}$ represents the volume change resulting from the photochemical processes such as cleavage of the Fe−CO bond, structural changes, solvation, and/or electrostriction. K is the instrument response parameter, and E_a is the number of Einsteins absorbed. To calibrate the instrument and eliminate the instrument response parameter, we measured the signal of a calorimetric reference under conditions identical to those used for the sample. The reference compound, Fe(III)4SP, does not undergo any photochemistry and releases absorbed energy into the surrounding solvent with a yield of unity. The amplitude of the reference acoustic signal, R, can then be expressed as

$$R = KE_aE_{h\nu}\left(\frac{\beta}{C_p\rho}\right) \quad (2)$$

where $E_{h\nu}$ is the energy of the photon at the excitation wavelength. To separate the contributions of the thermal and nonthermal volume changes to the acoustic signal, the acoustic traces were measured as a function of temperature in the temperature range from 16 to 35 °C. By taking the ratio of the amplitude of the sample and reference acoustic waves and plotting them as a function of the temperature-dependent term $[(C_p\rho)/\beta]$, according to eq 3, we can extrapolate the amount of heat released to the solution and the nonthermal volume change from the intercept and the slope of the linear plot, respectively.

$$\varphi E_{h\nu} = \left(\frac{S}{R}\right)E_{h\nu} = Q + \left(\frac{C_p\rho}{\beta}\right)\Delta V_{nonthermal} \quad (3)$$

For processes with a quantum yield, Φ, of <1, the reaction enthalpy (ΔH) and volume changes (ΔV) are determined according to eqs 4 and 5, respectively.

$$\Delta H = \frac{E_{h\nu} - Q}{\Phi} \quad (4)$$

$$\Delta V = \frac{\Delta V_{nonthermal}}{\Phi} \quad (5)$$

RESULTS

The steady-state absorption spectra of ferric, deoxy, and CO-bound His64Gln hNgb at pH 7 are displayed in Figure 2. The Fe^{3+}His64Gln mutant exhibits a Soret band at 408 nm, a pronounced visible band near 539 nm, and two additional

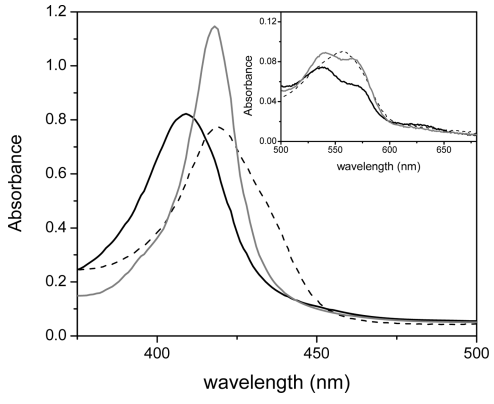

Figure 2. Steady-state absorption spectra of ferric (solid black line), ferrous (dashed black line), and CO-bound (solid gray line) H64Q Ngb. Conditions: 30 μM H64Q Ngb in 50 mM Tris buffer (pH 7.0).

bands at 575 and 630 nm. These band positions are identical to those observed for other Ngb His64 mutants[6,29] and similar to those observed in the spectra of other globins with a hexacoordinate high-spin Fe^{3+} heme iron having a weakly bound water molecule in the position of the axial ligand.[30] Analogous absorption spectra were reported for African elephant Mb with naturally occurring Gln64.[31] Reduction of the heme iron produces a bathochromic shift of the Soret band to 420 nm with a shoulder near 432 nm and an additional absorption band situated at 556 nm. This spectrum is similar to that reported for the His64Leu[4,32] and His64Val[33] mutants of Mb. The shoulder at 432 nm and the visible band at 556 nm are consistent with the pentacoordinate high-spin heme iron, whereas the Soret band maximum at 420 nm indicate the presence of a Ngb fraction with a hexacoordinate low-spin heme iron. Nienhaus et al.[32] have proposed that a water molecule or OH^- group may serve as a sixth axial ligand in the distal site of the His64Leu mutant in Fe^{2+}mNgb, whereas Uno et al.[34] have identified Lys67 as a possible sixth axial ligand at alkali pH. The CO-bound form of the His64Gln mutant exhibits a Soret band at 417 nm and α and β bands located at 567 and 539 nm, respectively, that are consistent with the formation of low-spin six-coordinate heme iron. The UV−vis spectra recorded for the His64Gln/Val68Phe double mutant are similar to those for His64Gln mutant, whereas the absorption spectra of Cys120Ser, Val68Phe, and Cys55Ser/Cys120Ser are identical to spectra of wild-type hNgb (data not shown).

Transient Absorption Spectroscopy. The kinetics for rebinding of the ligand to Ngb are more complex than those of binding of the diatomic ligand to pentacoordinate globins because of the hexacoordinate nature of Ngb and the heterogeneity of the heme group.[35] Previous studies have shown that CO rebinding is multiphasic, with geminate CO rebinding taking place on a nanosecond time scale and bimolecular rebinding of CO to the five-coordinate heme on the microsecond time scale.[23,36] Subsequent rebinding of CO to the six-coordinate bis-histidine heme is observed on the millisecond to second time scale, with the distal His dissociation representing the rate-limiting step.[35] Because the pentacoordinate and hexacoordinate Ngb species are in equilibrium, the ratio of the fast to slow phase of bimolecular CO rebinding can be modified by varying the ligand concentration and temperature. Under ligand saturation conditions and at ambient temperature, the fraction of the bis-histidine heme iron is negligible, and thus, only single-phase bimolecular rebinding of CO to five-coordinate heme iron is observed.[4,36]

Figure 3 shows TA traces on the nano- to microsecond time scale for rebinding of CO to five-coordinate Ngb WT and mutated proteins studied at 20 °C under CO saturating conditions (~1 mM CO). The geminate quantum yield (Φ_{gem}) was determined by taking the ratio of the amplitude of the absorbance change corresponding to the geminate process (A_{gem}) with respect to the total absorbance change (A_{total}) (Table 1), and the value determined for WT hNgb (Φ_{gem} = 0.32) matches well with the geminate quantum yield reported by Krielg et al. (Φ_{gem} = 0.32).[36] A large increase in Φ_{gem} was observed for Val68Phe Ngb (Φ_{gem} = 0.85) and for the double mutant His64Gln/Val68Phe (Φ_{gem} = 0.96).

The TA traces were analyzed using a multiexponential decay model:

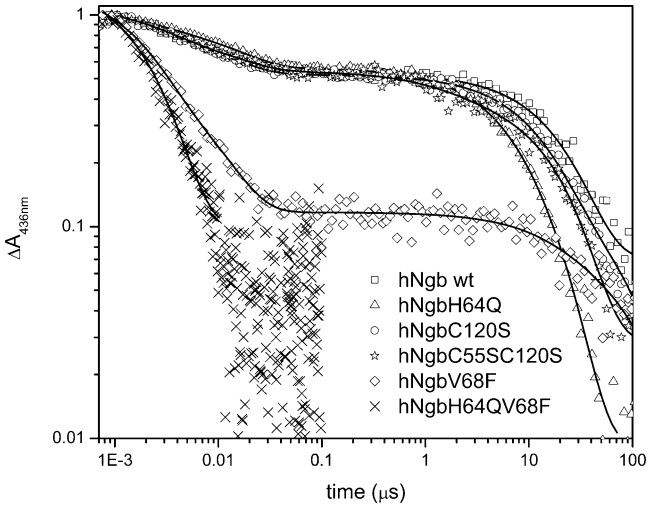

Figure 3. Transient absorption traces for CO geminate recombination and bimolecular rebinding to Ngbs. The initial amplitudes following the photodissociation of CO were normalized to 1. The solid lines correspond to a fit of experimental data using a four-exponential decay model. Conditions: 20 μM protein in 50 mM Tris buffer (pH 7.0) at 20 °C and 1 mM CO.

$$\left[\sum_i A_i \mathrm{e}\left(\frac{t}{\tau_i}\right)\right] \quad (6)$$

where τ_i and A_i correspond to the lifetime and amplitude for each kinetic step, respectively. CO geminate rebinding is found to be biphasic with the following rate constants for the fast and slow phases in the wild-type protein: k_{gem1} = (2.3 ± 0.8) × 10^8 s^{-1} and k_{gem2} = (3.4 ± 0.5) × 10^7 s^{-1}, respectively (Table 1). The observed rate constant for the slower geminate rebinding, k_{gem2}, matches well with that reported by Abbruzzetti et al.[23] Similar rate constants for CO geminate rebinding were resolved for other mutated proteins studied here except the His64Gln/Val68Phe double mutant for which only CO geminate rebinding with a single rate constant of (4.8 ± 0.3) × 10^8 s^{-1} was assessed. The observed heterogeneity reflects the fast ligand rebinding from the primary and secondary ligand docking sites that were identified by time-resolved IR spectroscopy.[37] The multiphasic CO geminate rebinding from alternative docking sites was also reported for CO geminate rebinding in hNgb encapsulated in silica gels,[23] although the fast rate constant reported here has not been resolved.

The bimolecular rebinding of CO to five-coordinate Ngb is also multiphasic for WT Ngb, with the rate constants for the fast and slow phases being 61 ± 7 μM^{-1} s^{-1} (~65%) and 9 ± 2 μM^{-1} s^{-1} (~35%), respectively. The biphasic bimolecular rebinding of CO to five-coordinate Ngb was observed previously and associated with the heterogeneous orientation of the heme group in Ngb.[35] The presence of two heme isomers was confirmed in an NMR study showing that the isomers are rotated by 180° and populated with a ratio of 2:1,[38] which matches the ratio of amplitudes for the fast and slow phases reported here.

The replacement of Cys120 with Ser or Val68 with Phe does not alter the rate of CO bimolecular rebinding. On the other hand, significantly faster CO bimolecular rebinding was observed for the His64Gln mutant with rate constants of 312 ± 24 and 95 ± 3 μM^{-1} s^{-1} exhibiting equal amplitudes. Similar acceleration for the CO bimolecular rebinding was observed in

dx.doi.org/10.1021/bi301016u | Biochemistry 2012, 51, 9984−9994

Table 1. Kinetic Parameters for Recombination of CO to Ngbs[a]

sample	k_{gem1} ($\times 10^8$ s^{-1})	k_{gem2} ($\times 10^7$ s^{-1})	k_{fast1} (μM^{-1} s^{-1})	k_{fast2} (μM^{-1} s^{-1})	k_{slow} (μM^{-1} s^{-1})	Φ_{gem}
WT	2.3 ± 0.8	3.4 ± 0.5	61 ± 7	9 ± 2	0.10 ± 0.01	0.32
His64Gln	3.8 ± 0.6	7.2 ± 0.9	312 ± 24	95 ± 3	–	0.32
Cys120Ser	5.0 ± 2.0	8.0 ± 3.0	90 ± 16	19 ± 7	0.09 ± 0.01	0.32
Cys55Ser/Cys120Ser	3.2 ± 0.5	4.7 ± 0.5	153 ± 31	29 ± 4	0.08 ± 0.01	0.32
Val68Phe	5.6 ± 0.4	10.9 ± 0.4	77 ± 36	9 ± 3	0.080 ± 0.01	0.85
His64Gln/Val68Phe	4.8 ± 0.3	–	–	–	–	0.96

[a]Rate constants (k_{gem} and k_{fast}) for binding of the ligand to five-coordinate Ngb were determined at 20 °C and 1 mM CO, whereas the slow phase was measured at 35 °C and 0.1 mM CO to increase the yield of bishistidyl Ngb.

the Cys120Ser/Cys55Ser double mutant with rate constants of 153 ± 31 μM^{-1} s^{-1} (~24%) and 29 ± 4 μM^{-1} s^{-1} (~76%) for the fast and slow phases of bimolecular association, respectively.

The pseudo-first-order rate constants for rebinding of CO to hexacoordinate bis-histidyl Ngb (k_{slow}) were determined under conditions that increase the population of bis-histidyl hNgb (35 °C and ~0.1 mM CO) (Table 1). Substitution of Val68 with Phe or Cys120 with Ser does not alter the rate constant for CO rebinding relative to that of the WT protein. The rate constant for rebinding of CO to bis-histidyl hNgb in the Cys55Ser/Cys120Ser double mutant (k_{slow} = 0.08 ± 0.01 μM^{-1} s^{-1}) is somewhat larger than the rate constant observed for the Cys55Ser single mutant (k_{slow} = 0.052 μM^{-1} s^{-1}).[20] Such an impact of the Cys120 mutation in the double mutant on the rate constant for rebinding of CO to bis-hisdidyl Fe^{2+}hNgb is surprising considering that this residue is located close to protein surface, approximately 18 Å from the heme binding pocket. Because the rate-limiting step for rebinding of CO to bis-histidyl Fe^{2+}hNgb is distal histidine dissociation, these data suggest that substitution of Cys120 with Ser leads to long-range structural changes that impact heme iron coordination.

PAC Measurements. An overlay of photoacoustic traces for photodissociation of CO from His64Gln hNgb and the reference compound, 4SP, is shown in Figure 4. The sample acoustic trace overlays in phase with the reference trace, indicating the absence of volume and/or enthalpy changes on the time scale between ~20 ns and ~5 μs. Similar photoacoustic time profiles were observed for the other mutated proteins investigated (data not shown). Plots of the PAC amplitude ratios as a function of the thermal coefficient $[(C_p\rho)/\beta]$ (see eq 3) over the temperature range of 16–35 °C are displayed in Figure 5. The reaction volume and enthalpy changes were determined using eqs 3–5 and are listed in Table 2. From the reaction volume change, the structural volume change, ΔV_{str}, that describes the difference between the partial molar volume of the five-coordinate Ngb and CO-bound Ngb can be determined according to the equation $\Delta V = V_{CO} + \Delta V_{str}$, where V_{CO} is the partial molar volume of CO (35 mL mol^{-1}).[27,39] The photodissociation of CO from WT hNgb is associated with a ΔV_{str} of −21.6 ± 0.9 mL mol^{-1}, and slightly more negative structural volume changes were observed for His64Gln and Cys120Ser proteins. Replacement of Val68 with

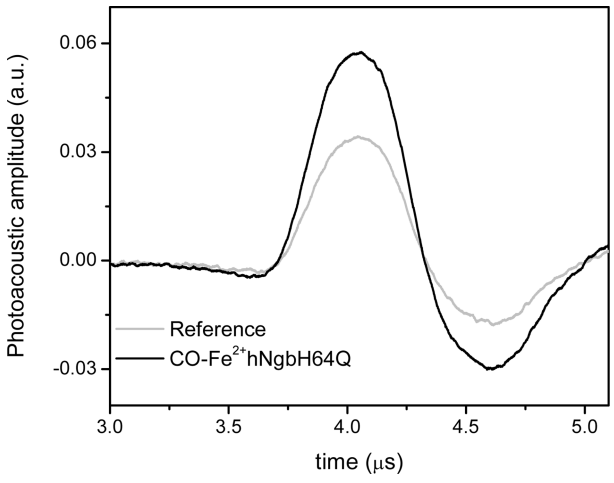

Figure 4. PAC traces for dissociation of CO from His64Gln Fe^{2+}hNgb (black line) and the reference compound, Fe(III)4SP (gray line), at 20 °C. Conditions: 20 μM His64Gln Ngb in 50 mM Tris buffer (pH 7.0) and 1 mM CO. The absorbance of the reference compound matched that of the sample at 532 nm.

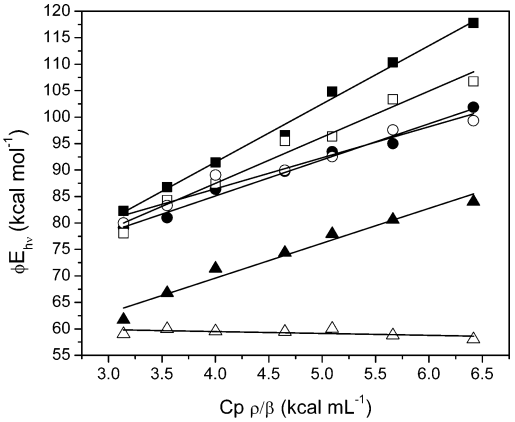

Figure 5. Plot of $\phi E_{h\nu}$ vs $(C_p\rho)/\beta$ for photodissociation of CO from wild-type Ngb (■), His64Gln (●), Val68Phe (△), Cys120Ser (○), Cys55Ser/Cys120Ser (□), and Cys55Ser (▲). The data for human Ngb and the C55S mutant were taken from ref 20. The corresponding volume and enthalpy changes were determined from the slope and intercept of the linear fits, respectively.

Table 2. Thermodynamic Parameters for Photodissociation of CO from Ngbs

	ΔH (kcal mol^{-1})	ΔV (mL mol^{-1})	ΔV_{str}[b] (mL mol^{-1})
wild type[a]	20 ± 4	13.4 ± 0.9	−21.6 ± 0.9
His64Gln	−6 ± 3	10.0 ± 0.5	−25.0 ± 0.5
Val68Phe	−48 ± 7	−2.4 ± 1.5	−37.4 ± 1.5
Cys120Ser	−3 ± 4	7.5 ± 0.6	−27.5 ± 0.6
Cys55Ser/Cys120Ser	−6 ± 4	12.2 ± 0.9	−22.5 ± 0.9

[a]From ref 20. [b]The structural volume change was determined using the equation $\Delta V_{str} = \Delta V - V_m^\circ$, where V_m° is the partial molar volume of CO (35 mL mol^{-1}).[27]

Phe has a significant impact on the structural volume change (ΔV_{str} = −37 ± 2 mL mol^{-1}) likely because of a larger structural reorganization of the distal pocket in this mutant. The overall enthalpy change for the photodissociation of CO from WT hNgb is 20 ± 4 kcal mol^{-1} and largely reflects the enthalpy of the Fe−CO bond energy.[20] Interestingly, all mutated proteins studied here exhibit negative enthalpy changes for CO photolysis with a ΔH of −3 ± 4 kcal mol^{-1} for the Cys120Ser mutant and −48 ± 7 kcal mol^{-1} for the Val68Phe mutant. We did not characterize volume and enthalpy changes associated with photodissociation of CO from the double mutant His64Gln/Val68Phe, because the quantum yield for geminate recombination is close to unity.

DISCUSSION

Role of Distal Residues His64 and Val68 in Controlling Ligand Migration in Ngb. Conserved distal pocket residues His64 and Val68 play a crucial role in regulating the affinity for diatomic ligands in vertebral globins. In Ngb, His64 modulates the affinity for CO and O_2,[4,12] is responsible for the pH dependence of O_2 binding,[25] and protects against formation of tyrosine−phenoxyl radicals in the presence of hydrogen peroxide.[40] Here we show that the replacement of His64 with a polar Gln residue of a comparable size moderately alters the rate for bimolecular rebinding of CO to the five-coordinate hNgb with the rate constant being approximately 5 and 10 times larger than the rate constant for the fast and slow bimolecular rebinding in WT, respectively. A similar increase in the rate constant for the fast phase of bimolecular rebinding was reported previously for the His64Gln substitution by Hamdane et al. (k_{fast} = 290 μM^{-1} s^{-1})[19] and by others for hNgb mutants with a Leu (k_{fast} = 237 μM^{-1} s^{-1})[29] or Val (k_{fast} = 230 μM^{-1} s^{-1})[4] residue in position 64. In those studies, the heterogeneous rebinding of CO to the five-coordinate heme iron was also detected; however, the rate constant for the slow phase was not reported. The biphasic rebinding of CO to the His64Val mutant was observed at pH 9.5 with rate constants similar to those reported here (k_{fast1} = 350 μM^{-1} s^{-1}, and k_{fast2} = 45 μM^{-1} s^{-1}); however, the authors assigned the slower process to the partial coordination of Lys67.[34] On the basis of the mNgb crystal structure, it was proposed that binding of CO to the heme iron requires the distal histidine side chain swinging out of the distal pocket and a concomitant breakage of the electrostatic/hydrogen bonding network among Lys67, heme 7-propionate, and Tyr44. Substitution of distal His with Gln opens the access to the distal pocket, resulting in a lowering of the activation barrier for exogenous ligand binding.

The relatively moderate impact of the His64 side chain on the ligand migration within the protein matrix is evident from the quantum yield value for the CO geminate rebinding that is identical to that measured for WT hNgb (Φ_{gem} = 0.32). In comparison, an analogous replacement in swMb results in a substantial increase in the amplitude for CO geminate rebinding (Φ_{gem} ∼ 0.04 in WT Mb, and Φ_{gem} = 0.67 in the His64Gln Mb mutant).[41] These results show that in Ngb the residue occupying position 64 does not influence the migration of the ligand between the heme distal pocket and adjacent hydrophobic cavities and/or escape to the surrounding solvent.

The replacement of Val68 with Phe, on the other hand, significantly increases the amplitude for geminate CO rebinding (Φ_{gem} = 0.85), indicating that the presence of the bulky benzyl side chain at position 68 introduces a steric block for CO migration between the distal pocket and the internal hydrophobic cavities. This is further supported by the study of the His64Gln/Val68Phe double mutant in which the escape of the photodissociated ligand into the surrounding solvent is nearly completely hindered, which is evident from the geminate quantum yield approaching unity. Interestingly, the impact of the His64 and Val68 mutation on the CO geminate process is not additive, suggesting that the simultaneous mutation of both distal residues leads to a reorganization of the volume and/or dynamics of the heme distal pocket and/or nearby internal cavities. In Ngb, Val68 and the other conserved hydrophobic residues, Leu27, Val109, and Leu113, surround the Xe_4 cavity that is located in a position analogous to that in Mb.[22] Yin et al.[42] have probed the structure of the heme binding site in the His64Gln/Val68Phe hNgb double mutant using solution ^{1}H NMR. They reported that the Phe side chain adopts a spatial orientation similar to that found in the structure of the Mb triple mutant (H64Q/L29F/V64F),[43] with the side chain blocking the Xe_4 cavity. The reduction of the volume in the Xe_4 cavity thus results in an efficient blockage of migration of CO between the distal pocket and adjacent hydrophobic cavities, confirming that the residue at position 68 exhibits an analogous functional role in both Ngb and pentacoordinate vertebrate globins.[44]

The mutation of distal residue His64 or Val68 significantly alters the thermodynamics of structural changes associated with ligand photorelease. The photorelease of CO from WT hNgb is endothermic (ΔH = 20 ± 4 kcal mol^{-1}) and associated with a negative structural volume change (ΔV = −21.6 ± 0.9 mL mol^{-1}).[20] In the structure of WT Fe^{2+}mNgb, a water molecule was resolved in the vicinity of the distal histidine that is missing in the structure of CO-bound Fe^{2+}mNgb. The internal water molecule (Wat9 in PDB entry 1Q1F) is surrounded by the side chains of three Phe residues (Phe28, Phe42, and Phe61) and stabilized within the protein matrix through a hydrogen bond with the His64 side chain, the carbonyl oxygen of Phe61, and weak hydrogen bonds to the hydroxyl group of Tyr44 and the carbonyl oxygen of Glu60. The negative structural volume change determined for photodissociation of CO from WT hNgb is consistent with the fast uptake of a water molecule that is concomitant with the escape of CO from the protein matrix. This is further supported by the absolute magnitude of the structural volume change that is similar to the partial molar volume of water (V_m° = 18 mL mol^{-1}). Because the water molecule forms hydrogen bonds with nearby amino acid residues, the uptake into the protein matrix does not result in a significant enthalpy change, and the observed enthalpy of 20 kcal mol^{-1} corresponds to the photodissociation of the Fe−CO bond. Xu et al.[45] have proposed that an electrostatic/hydrogen bonding network formed by Lys67, Tyr44, His64, and heme 7-propionate stabilizes the heme group within the heme binding pocket and CO association leads to the weakening of electrostatic interactions, including the breakage of the salt bridge between Lys67 and heme propionate. The enthalpy change associated with the destabilization of such polar network was estimated to be relatively small, ∼1.7 kcal mol^{-1},[46,47] and does not significantly contribute to the observed enthalpy change.[14] In addition to Fe^{2+}hNgb hydration, other factors such as sliding of the heme group and reshaping of the internal hydrophobic cavities may contribute to the observed volume and/or enthalpy change. However, the impact of these perturbations on the structural volume change is likely to be small as these changes are localized within the protein matrix

and thus do not impact the overall protein structure and/or charge distribution on the protein surface.

The photodissociation of CO from the His64Gln mutant is exothermic ($\Delta H = -6 \pm 3$ kcal mol^{-1}) and accompanied by a negative structural volume change of -25.0 ± 0.5 mL mol^{-1}. More negative volume and enthalpy changes are observed for photorelease of CO from the Val68Phe mutant ($\Delta H = -48 \pm 7$ kcal mol^{-1}, and $\Delta V_{str} = -37.4 \pm 1.5$ mL mol^{-1}). The negative enthalpy change for photorelease of CO from hNgb mutants indicates that the corresponding rebinding of CO to five-coordinate hNgb is endothermic and entropically driven. A comparable positive enthalpy for binding of O_2 to hNgb was observed by Fago et al.[25] They reported that the hNgb oxygenation is endothermic ($\Delta H = 12.7$ kcal mol^{-1}) below 18 °C and becomes exothermic at higher temperatures ($\Delta H = -15.7$ kcal mol^{-1}). They attributed the exothermic ligand binding to the weakening of the electrostatic/hydrogen bonding interactions among His64, Lys67, and heme 7-propionate at high temperatures. At low temperatures, stronger polar interactions contribute to the observed positive enthalpy for oxygen binding. The negative reaction enthalpy observed for photorelease of CO from His64Gln Fe^{2+}hNgb suggests that substitution of His64 promotes a reorganization of the electrostatic/hydrogen bonding network in the vicinity of the heme 7-propionate group in a manner similar to that observed for binding of oxygen to hNgb below 18 °C. Indeed, this network of polar residues that also includes Tyr44 and a water molecule is not rigid as evident from an overlay of mNgb and hNgb structures. For example, Lys67 forms a hydrogen bond with the heme 7-propionate in the structure of Fe^{3+}mNgb (PDB entry 1Q1F), whereas in the structure of CO-bound mNgb and Fe^{2+}mNgb (PBD entries 1W92 and 2VRY, respectively), the Lys67 side chain is positioned within hydrogen bonding distance of both heme 6- and 7-propionate group. Tyr44 is located in the highly flexible CD region (residues 40−60), and its side chain was not resolved in two molecules of Fe^{3+}hNgb (PDB entry 1OJ6), pointing toward an increased flexibility of this residue in hNgb. In addition, computational studies have revealed that the solvent accessible area of Tyr44 increases in the CO-bound form of the His64Val mutant relative to that of the WT protein, confirming that the distal His mutation alters this electrostatic network.[45] These results suggest that the electrostatic/hydrogen bond network can be relatively easily reorganized either by changes in the temperature or by a single-residue substitution. Xu et al.[45] have proposed that the electrostatic/hydrogen bonding network between the heme propionate groups and the apoprotein stabilizes the position of the prosthetic group and modulates the heme sliding mechanism in Ngb. Therefore, the impact of the His64Gln substitution on the energetics of association of CO with five-coordinate hNgb may be the result of the altered heme sliding mechanism in this mutated protein.

Other factors may also contribute to the observed negative enthalpy change for CO photorelease. The UV−vis spectra revealed a small fraction of six-coordinate heme iron in Fe^{2+}Ngb mutants lacking His64 likely because of the presence of a water molecule in the sixth axial position.[36] Although a water molecule associated with the reduced heme iron is unusual in globins, the ferrous aquo−Mb complex was detected only below 150 K.[48] Strickland et al.[49] have reported that binding of a water molecule to the heme model complexes of Fe^{2+} heme involves a low energy barrier, and it is energetically favorable by ∼10 kcal mol^{-1}. In the His64Gln mutant, the association of a water molecule with the ferrous heme may be facilitated by the presence of a highly reactive heme iron, which is evident from the faster kinetics for rebinding of CO to the five-coordinate heme iron compared to that of WT hNgb and possibly by the increased accessibility to the sixth axial position of the heme ferrous iron because of the replacement of the His64 imidazole ring with Gln. More negative enthalpy and structural volume changes for photodissociation of CO from the Val68Phe mutant relative to the His64Gln mutant point toward a significant reorganization of the heme distal pocket and surrounding hydrophobic cavities and/or an altered mechanism of interactions of diatomic ligands with heme iron in the Val68Phe mutant. In the absence of a crystal structure for the Val68Phe mutant, it is difficult to pinpoint structural factors that contribute to the observed thermodynamic parameters. The large negative structural volume change ($\Delta V_{str} = -37.4 \pm 1.5$ mL mol^{-1}) and the exothermic enthalpy change ($\Delta H = -48 \pm 7$ kcal mol^{-1}) observed for photorelease of CO from the Val68Phe mutant are consistent with a reorganization of charges, including salt bridges associated with the transition between the CO-bound hNgb and Fe^{2+}hNgb that is not present in the WT protein.

Role of the Cys Residues in Controlling Ligand Migration in hNgb. The two cysteine residues examined here, Cys55 and Cys120, are well-conserved among mammalian Ngbs. Replacement of Cys120 with Ser does not alter the kinetics of geminate rebinding or bimolecular rebinding of CO to pentacoordinate Fe^{2+}hNgb, consistent with the position of Cys120 being near the protein surface and ∼19 Å from the heme iron. On the other hand, bimolecular rebinding of CO to the five-coordinate iron in the Cys55Ser/Cys120Ser hNgb double mutant is faster than in the WT protein and displays an acceleration similar to that observed for the His64Gln mutant. This result is somehow surprising because no acceleration for bimolecular CO rebinding was observed for the Cys55Ser hNgb single mutant,[20] suggesting that simultaneous replacement of Cys120 and Cys55 leads to global structural changes that impact the rate of CO bimolecular rebinding.

The reaction enthalpy changes determined for photodissociation of CO from the Cys120Ser mutant and Cys55Ser/Cys120Ser double mutant are comparable and close to 0 kcal mol^{-1}. On the other hand, the structural volume change measured for the Cys120Ser mutant is ∼6 mL mol^{-1} more negative than that measured for the WT protein, whereas a similar structural volume change was observed for the Cys55Ser/Cys120Ser double mutant. Previously, we reported that the single Cys55Ser mutation in hNgb does not alter the enthalpy change associated with photorelease of CO from Ngb,[20] pointing out that the replacement of Cys120 with Ser leads to a decrease in the reaction enthalpy change of ∼20 kcal mol^{-1}. In the crystal structure of CO-bound mNgb with both Cys55 and Cys120 replaced with Ser, the hydroxyl group of Ser120 is located at the end of helix G and forms a hydrogen bond to the carbonyl oxygen of Met116, whereas in the Fe^{2+}mNgb structure, the Ser120 side chain populates two conformations. One conformation corresponds to that found in the CO-bound Fe^{2+}Ngb structure, whereas the second conformation shows the Ser120 side chain rotated by 124°, forming a hydrogen bond with His23 from helix B. In the Fe^{2+}mNgb structure, the side chain of His23 is involved in a larger hydrogen bonding network that includes Glu22 and Ser19 that is part of the A−B loop, whereas the hydrogen bond between Glu22 and His23 is missing in CO-bound mNgb

(Figure 6). Thus, we propose that in the mutants carrying a Ser residue at position 120, escape of CO from the protein matrix is

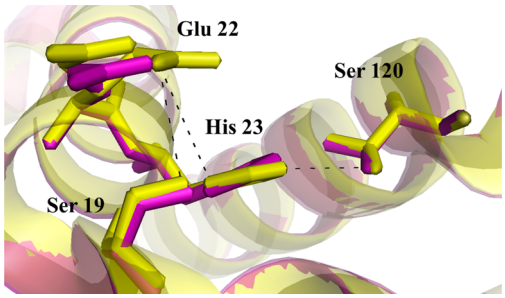

Figure 6. Positions of Ser120, His23, Glu22, and Ser19 in the structure of CO-bound mNgb (purple, PDB entry 1W92) and in the structure of Fe^{2+}mNgb (yellow, PDB entry 2VRY). The hydrogen bond network connecting helix G and the loop between helices A and B in the Fe^{2+}mNgb form (black lines) is missing in the structure of CO-bound mNgb.

associated with the fast (τ < 50 ns) formation of a hydrogen bond network involving Ser120, His23, and Glu22 that leads to the negative enthalpy change observed for photodissociation of CO for the Cys120Ser mutant and the Cys120Ser double mutant. In WT Ngb that carries a Cys residue at position 120, this hydrogen bonding network is missing and the observed positive enthalpy change of 20 kcal mol^{-1} represents the scission of the Fe−CO bond. These data also indicate that migration of CO between the protein matrix and the surrounding solvent results in reorganization of the interface between helix G and the A−B loop, and this interface may facilitate escape of the photodissociation ligand from the protein matrix. The analysis of the ligand migration pathways in Ngb was addressed in several computational studies. Anselmi et al.[24] have reported that a significant fraction of the photodissociated CO molecules cross the Xe_4 cavity region and escape through a phantom 1 site between helix G and the A−B loop, in excellent agreement with our experimental data. The A−B loop was also identified as a ligand transition pathway for escape of CO from the Ngb, named exit 3, by Bocahut et al.,[18] although they associated this pathway with escape of CO from hNgb with the reduced disulfide bound.

The molecular mechanism of ligand migration and the role of internal hydrophobic cavities were intensively studied in Mb using time-resolved absorption/IR spectroscopy, time-resolved X-ray crystallography, and computational studies in combination with site-directed mutagenesis.[50−54] The schematic description of the ligand migration pathways in Mb and Ngb is presented in Scheme 1. The ligand migration in Mb can be described using a side path kinetic scheme.[50] Upon photocleavage of the Fe−CO bond, the photoreleased ligand rapidly

Scheme 1

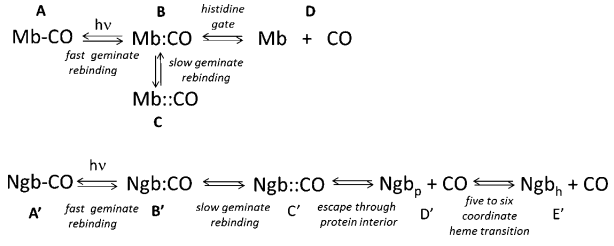

translates into the primary docking site located above the heme iron plane (state B) where it remains for <30 ns.[55] Subsequently, the CO molecule can either rebind to the heme iron through a geminate rebinding process, escape into the surrounding solvent (state D) through the so-called "histidine gate", or migrate into one of the nearby hydrophobic cavities, Xe_4 or Xe_1 site (state C). To escape from the protein matrix, the photodissociated ligand transiently located within the hydrophobic cavities has to return to primary docking site B and then leave through the histidine gate.

The internal ligand migration is directed by the conformational changes of amino acid side chains located at the solvent interface and in the proximity of site B, including I28, L29, L32, F43, F46, F64, V68, and I 107.[52] For example, substitution of Leu29 with Trp blocks geminate rebinding as well as escape of the photodissociated ligand through the His gate and promotes ligand trapping in the Xe_4 or Xe_1 cavity. On the other hand, replacement of distal His64 with a nonpolar residue such as Leu or Val increases the rate of CO bimolecular rebinding as well as the geminate rebinding yield (Φ_{gem} = 0.37 or 0.34, respectively), and a significantly larger increase in the rate of geminate rebinding was observed for the His64Gln mutant (Φ_{gem} = 0.67).[41] The effect of replacement of the Val68 side chain with aromatic side chains on the ligand migration pathway was probed by several groups demonstrating that the presence of a bulky side chain at position 68 results in a trapping of photodissociated ligands within docking site B and inhibition of the transition of the ligand into more remote sites, particularly the Xe_4 cavity.[52,56−58] Simultaneous alteration of both His64 and Val68 side chains effectively blocks escape of CO from the protein matrix, resulting in a large geminate quantum yield.[59]

On the basis of the kinetic and photothermal data presented here and previous spectroscopic and computational results, we propose an alternative pathway for ligand migration in Ngb. After Fe−CO bond photocleavage, the ligand diffuses into the primary docking site (state B′) that was shown to consist of two sites: B_1′ surrounded by Phe28, Leu31, and Phe32 and site B_2′ surrounded by Phe28, His64, and Val68. The subsequent transition includes ligand migration into the Xe_4 hydrophobic cavity (state C′) that is facilitated by a low energy barrier, ∼1.1 kJ mol^{-1}, between sites B′ and C′.[32] As in Mb, the ligand migration between states B′ and C′ is gated by the side chain of Val68, which is evident from the increased rate of CO geminate rebinding in the Val68Phe mutant. The alteration of the His64 side chain has an only minor impact on the ligand transition between the distal pocket and site C′, suggesting that in Ngb the His64 side chain does not regulate diffusion of the ligand between internal cavities or block escape of the ligand from the protein matrix.

The exact pathway for escape of the ligand from state C′ remains unclear. On the basis of the crystal structure of deoxy-mNgb and CO-bound mNgb, it was suggested that the wide hydrophobic tunnel connecting the distal pocket with the surrounding solvent in the deoxy protein provides an effective pathway for ligand migration.[13] Indeed, the Xe_4 hydrophobic site is located in the vicinity of the hydrophobic tunnel entrance, indicating that the arrival of the ligand in the tunnel is regulated by the Val68 side chain. The results presented here demonstrate that the thermodynamic parameters associated with CO escape are altered by the hydrogen bond network connecting helix G and the loop between helices A and B, suggesting that this region may serve as a ligand migration

dx.doi.org/10.1021/bi301016u | *Biochemistry* 2012, 51, 9984−9994

pathway in hNgb as was previously proposed by Anselmi et al.[24] Alternatively, the rearrangement of the region between helix G and the A−B loop can be a part of the larger conformational transition between the ligand-bound and ligand free Ngb, including the reshaping of the internal hydrophobic tunnel that provides an effective ligand escape pathway. Finally, following escape of CO to the solvent (state D′), the Ngb structure undergoes a considerable reorganization that involves the heme repositioning and the re-formation of the Fe−His64 coordination bond (state E′) occurring on a 100 ms time scale.

CONCLUSION

In summary, our PAC results in combination with transient absorption studies reveal that escape of the ligand from the protein matrix in hNgb is significantly faster than in Mb, suggesting that in hNgb the histidine gate mechanism does not regulate the ligand escape between the distal pocket and the surrounding solvent. On the other hand, the highly conserved Val68 residue appears to have an analogous role in hNgb and in vertebrate five-coordinate globins and regulates the internal movement of the photodissociated ligand between the heme distal pocket and surrounding hydrophobic cavities. The thermodynamic data for photodissociation of the ligand from mutated proteins with Cys120 replaced with Ser indicate that the interface between helix G and the A−B loop may provide a pathway for the migration of CO from the internal hydrophobic cavities to the protein exterior. The electrostatic/hydrogen bond network between the heme propionate groups and the apoprotein not only stabilizes the prosthetic group but also influences thermodynamics of binding of the diatomic ligand to heme iron and to some extent provides a barrier for rebinding of the diatomic ligand to the five-coordinate Ngb. Altogether, these data confirm a distinct mechanism of interaction of hNgb with diatomic ligands compared to other vertebrate globins such as myoglobin and hemoglobin.

AUTHOR INFORMATION

Corresponding Author

*Department of Chemistry and Biochemistry, Florida International University, 11200 SW 8th St., Miami, FL 33199. Phone: (305) 348-7406. Fax: (305) 348-3772. E-mail: miksovsk@fiu.edu.

Funding

This work was supported by the National Science Foundation (Grant MCB 10218 31 to J.M.) and the J. & E. Biomedical Research Program (Florida Department of Health) (J.M.).

Notes

The authors declare no competing financial interest.

ACKNOWLEDGMENTS

We would like to thank to Vladislav Lukyanchenko from Ultrafast Systems, LLC, for the assistance with nanosecond transient spectroscopy measurements.

ABBREVIATIONS

DTT, dithiothreitol; Fe(III)4SP, iron(III) tetraphenylsulfonatoporphyrin; hNgb, human neuroglobin; mNgb, mouse neuroglobin; PAC, photoacoustic calorimetry; PDB, Protein Data Bank; rNgb, rat neuroglobin; TA, transient absorption.

REFERENCES

(1) Burmester, T., Weich, B., Reinhardt, S., and Hankeln, T. (2000) A vertebrate globin expressed in the brain. *Nature 407*, 520−523.

(2) Sun, Y., Jin, K., Mao, X. O., Zhu, Y., and Greenberg, D. A. (2001) Neuroglobin is up-regulated by and protects neurons from hypoxic-ischemic injury. *Proc. Natl. Acad. Sci. U.S.A. 98*, 15306−15311.

(3) Sun, Y., Jin, K., Peel, A., Mao, X. O., Xie, L., and Greenberg, D. A. (2003) Neuroglobin protects the brain from experimental stroke in vivo. *Proc. Natl. Acad. Sci. U.S.A. 100*, 3497−3500.

(4) Dewilde, S., Kiger, L., Burmester, T., Hankeln, T., Baudin-Creuza, V., Aerts, T., Marden, M. C., Caubergs, R., and Moens, L. (2001) Biochemical characterization and ligand binding properties of neuroglobin, a novel member of the globin family. *J. Biol. Chem. 276*, 38949−38955.

(5) Wakasugi, K., Nakano, T., and Morishima, I. (2003) Oxidized human neuroglobin acts as a heterotrimeric gα protein guanine nucleotide dissociation inhibitor. *J. Biol. Chem. 278*, 36505−36512.

(6) Van Doorslaer, S., Dewilde, S., Kiger, L., Nistor, S. V., Goovaerts, E., Marden, M. C., and Moens, L. (2003) Nitric oxide binding properties of neuroglobin. A characterization by EPR and flash photolysis. *J. Biol. Chem. 278*, 4919−4925.

(7) Herold, S., Fago, A., Weber, R. E., Dewilde, S., and Moens, L. (2004) Reactivity studies of the Fe(III) and Fe(II)NO forms of human neuroglobin reveal a potential role against oxidative stress. *J. Biol. Chem. 279*, 22841−22847.

(8) Fago, A., Mathews, A. J., Moens, L., Dewilde, S., and Brittain, T. (2006) The reaction of neuroglobin with potential redox protein partners cytochrome b5 and cytochrome c. *FEBS Lett. 580*, 4884−4888.

(9) Brittain, T., Skommer, J., Henty, K., Birch, N., and Raychaudhuri, S. (2010) A role for human neuroglobin in apoptosis. *IUBMB Life 62*, 878−885.

(10) Wakasugi, K., Takahashi, N., Uchida, H., and Watanabe, S. (2011) Species-specific functional evolution of neuroglobin. *Mar. Genomics 4*, 137−142.

(11) Brittain, T., Skommer, J., Raychaudhuri, S., and Birch, N. (2010) An antiapoptotic neuroprotective role for neuroglobin. *Int. J. Mol. Sci. 11*, 2306−2321.

(12) Pesce, A., Dewilde, S., Nardini, M., Moens, L., Ascenzi, P., Hankeln, T., Burmester, T., and Bolognesi, M. (2003) Human brain neuroglobin structure reveals a distinct mode of controlling oxygen affinity. *Structure 11*, 1087−1095.

(13) Vallone, B., Nienhaus, K., Matthes, A., Brunori, M., and Nienhaus, G. U. (2004) The structure of carbonmonoxy neuroglobin reveals a heme-sliding mechanism for control of ligand affinity. *Proc. Natl. Acad. Sci. U.S.A. 101*, 17351−17356.

(14) Vallone, B., Nienhaus, K., Brunori, M., and Nienhaus, G. (2004) The structure of murine neuroglobin: Novel pathways for ligand migration and binding. *Proteins: Struct., Funct., Bioinf. 56*, 85−92.

(15) Arcovito, A., Moschetti, T., D'Angelo, P., Mancini, G., Vallone, B., Brunori, M., and Della Longa, S. (2008) An X-ray diffraction and X-ray absorption spectroscopy joint study of neuroglobin. *Arch. Biochem. Biophys. 475*, 7−13.

(16) Trent, J. T., III, Watts, R. A., and Hargrove, M. S. (2001) Human neuroglobin, a hexacoordinate hemoglobin that reversibly binds oxygen. *J. Biol. Chem. 276*, 30106−30110.

(17) Nadra, A. D., Marti, M. A., Pesce, A., Bolognesi, M., and Estrin, D. A. (2008) Exploring the molecular basis of heme coordination in human neuroglobin. *Proteins 71*, 695−705.

(18) Bocahut, A., Bernad, S., Sebban, P., and Sacquin-Mora, S. (2009) Relating the diffusion of small ligands in human neuroglobin to its structural and mechanical properties. *J. Phys. Chem. B 113*, 16257−16267.

(19) Hamdane, D., Kiger, L., Dewilde, S., Green, B. N., Pesce, A., Uzan, J., Burmester, T., Hankeln, T., Bolognesi, M., Moens, L., and Marden, M. C. (2003) The redox state of the cell regulates the ligand binding affinity of human neuroglobin and cytoglobin. *J. Biol. Chem. 278*, 51713−51721.

(20) Astudillo, L., Bernad, S., Derrien, V., Sebban, P., and Miksovska, J. (2010) Probing the role of the internal disulfide bond in regulating conformational dynamics in neuroglobin. *Biophys. J. 99*, L16−L18.
(21) Ezhevskaya, M., Trandafir, F., Moens, L., Dewilde, S., and Van Doorslaer, S. (2011) EPR investigation of the role of B10 phenylalanine in neuroglobin: Evidence that B10Phe mediates structural changes in the heme region upon disulfide-bridge formation. *J. Inorg. Biochem. 105*, 1131−1137.
(22) Moschetti, T., Mueller, U., Schulze, J., Brunori, M., and Vallone, B. (2009) The structure of neuroglobin at high Xe and Kr pressure reveals partial conservation of globin internal cavities. *Biophys. J. 97*, 1700−1708.
(23) Abbruzzetti, S., Faggiano, S., Bruno, S., Spyrakis, F., Mozzarelli, A., Dewilde, S., Moens, L., and Viappiani, C. (2009) Ligand migration through the internal hydrophobic cavities in human neuroglobin. *Proc. Natl. Acad. Sci. U.S.A. 106*, 18984−18989.
(24) Anselmi, M., Di Nola, A., and Amadei, A. (2011) Kinetics of carbon monoxide migration and binding in solvated neuroglobin as revealed by molecular dynamics simulations and quantum mechanical calculations. *J. Phys. Chem. B 115*, 2436−2446.
(25) Fago, A., Hundahl, C., Dewilde, S., Gilany, K., Moens, L., and Weber, R. E. (2004) Allosteric regulation and temperature dependence of oxygen binding in human neuroglobin and cytoglobin: Molecular mechanisms and physiological significance. *J. Biol. Chem. 279*, 44417−44426.
(26) Miksovska, J., Yom, J., Diamond, B., and Larsen, R. W. (2006) Spectroscopic and photothermal study of myoglobin conformational changes in the presence of sodium dodecyl sulfate. *Biomacromolecules 7*, 476−482.
(27) Larsen, R. W., and Miksovska, J. (2007) Time resolved thermodynamics of ligand binding to heme proteins. *Coord. Chem. Rev. 251*, 1101−1127.
(28) Gensch, T., and Viappiani, C. (2003) Time-resolved photothermal methods: Accessing time-resolved thermodynamics of photoinduced processes in chemistry and biology. *Photochem. Photobiol. Sci. 2*, 699−721.
(29) Nienhaus, K., Kriegl, J. M., and Nienhaus, G. U. (2004) Structural dynamics in the active site of murine neuroglobin and its effects on ligand binding. *J. Biol. Chem. 279*, 22944−22952.
(30) Quillin, M., Arduini, R., Olson, J., and Phillips, G. (1993) High-resolution crystal-structures of distal histidine mutants of sperm whale myoglobin. *J. Mol. Biol. 234*, 140−155.
(31) Tada, T., Watanabe, Y., Matsuoka, A., Ikeda-Saito, M., Imai, K., Ni-hei, Y., and Shikama, K. (1998) African elephant myoglobin with an unusual autoxidation behavior: Comparison with the H64Q mutant of sperm whale myoglobin. *Biochim. Biophys. Acta 1387*, 165−176.
(32) Nienhaus, K., Lutz, S., Meuwly, M., and Nienhaus, G. U. (2010) Structural identification of spectroscopic substates in neuroglobin. *ChemPhysChem 11*, 119−129.
(33) Tiso, M., Tejero, J., Basu, S., Azarov, I., Wang, X., Simplaceanu, V., Frizzell, S., Jayaraman, T., Geary, L., Shapiro, C., Ho, C., Shiva, S., Kim-Shapiro, D. B., and Gladwin, M. T. (2011) Human neuroglobin functions as a redox-regulated nitrite reductase. *J. Biol. Chem. 286*, 18277−18289.
(34) Uno, T., Ryu, D., Tsutsumi, H., Tomisugi, Y., Ishikawa, Y., Wilkinson, A. J., Sato, H., and Hayashi, T. (2004) Residues in the distal heme pocket of neuroglobin. Implications for the multiple ligand binding steps. *J. Biol. Chem. 279*, 5886−5893.
(35) Kiger, L., Uzan, J., Dewilde, S., Burmester, T., Hankeln, T., Moens, L., Hamdane, D., Baudin-Creuza, V., and Marden, M. (2004) Neuroglobin ligand binding kinetics. *IUBMB Life 56*, 709−719.
(36) Kriegl, J. M., Bhattacharyya, A. J., Nienhaus, K., Deng, P., Minkow, O., and Nienhaus, G. U. (2002) Ligand binding and protein dynamics in neuroglobin. *Proc. Natl. Acad. Sci. U.S.A. 99*, 7992−7997.
(37) Nienhaus, K., and Nienhaus, G. (2005) A spectroscopic study of structural heterogeneity and carbon monoxide binding in neuroglobin. *J. Biol. Phys. 31*, 417−432.
(38) Du, W., Syvitski, R., Dewilde, S., Moens, L., and La Mar, G. N. (2003) Solution ^{1}H NMR characterization of equilibrium heme orientational disorder with functional consequences in mouse neuroglobin. *J. Am. Chem. Soc. 125*, 8080−8081.
(39) Hara, T., Hirota, N., and Terazima, M. (1996) New application of the transient grating method to a photochemical reaction: The enthalpy, reaction volume change, and partial molar volume measurements. *J. Phys. Chem. 100*, 10194−10200.
(40) Lardinois, O. M., Tomer, K. B., Mason, R. P., and Deterding, L. J. (2008) Identification of protein radicals formed in the human neuroglobin-H_2O_2 reaction using immuno-spin trapping and mass spectrometry. *Biochemistry 47*, 10440−10448.
(41) Lambright, D., Balasubramanian, S., Decatur, S., and Boxer, S. (1994) Anatomy and dynamics of a ligand-binding pathway in myoglobin: The roles of residues 45, 60, 64, and 68. *Biochemistry 33*, 5518−5525.
(42) Yin, G., Li, Y., Li, J., Li, J., Du, W., Wei, Q., and Fang, W. (2008) Solution ^{1}H NMR study of the active site structure for the double mutant H64Q/V68F cyanide complex from mouse neuroglobin. *Biophys. Chem. 136*, 115−123.
(43) Nguyen, B., Zhao, X., Vyas, K., La Mar, G., Lile, R., Brucker, E., Phillips, G., Olson, J., and Wittenberg, J. (1998) Solution and crystal structures of a sperm whale myoglobin triple mutant that mimics the sulfide-binding hemoglobin from lucina pectinata. *J. Biol. Chem. 273*, 9517−9526.
(44) Dantsker, D., Roche, C., Samuni, U., Blouin, G., Olson, J., and Friedman, J. (2005) The position 68(E11) side chain in myoglobin regulates ligand capture, bond formation with heme iron, and internal movement into the xenon cavities. *J. Biol. Chem. 280*, 38740−38755.
(45) Xu, J., Yin, G., and Du, W. (2011) Distal mutation modulates the heme sliding in mouse neuroglobin investigated by molecular dynamics simulation. *Proteins: Struct., Funct., Bioinf. 79*, 191−202.
(46) Horovitz, A., Serrano, L., Avron, B., Bycroft, M., and Fersht, A. (1990) Strength and cooperativity of contributions of surface salt bridges to protein stability. *J. Mol. Biol. 216*, 1031−1044.
(47) Takano, K., Tsuchimori, K., Yamagata, Y., and Yutani, K. (2000) Contribution of salt bridges near the surface of a protein to the conformational stability. *Biochemistry 39*, 12375−12381.
(48) Lamb, D., Ostermann, A., Prusakov, V., and Parak, F. (1998) From metmyoglobin to deoxymyoglobin: Relaxations of an intermediate state. *Eur. Biophys. J. 27*, 113−125.
(49) Strickland, N., and Harvey, J. N. (2007) Spin-forbidden ligand binding to the ferrous-heme group: Ab initio and DFT studies. *J. Phys. Chem. B 111*, 841−852.
(50) Olson, J. S., Soman, J., and Phillips, G. N., Jr. (2007) Ligand pathways in myoglobin: A review of Trp cavity mutations. *IUBMB Life 59*, 552−562.
(51) Brunori, M., and Gibson, Q. (2001) Cavities and packing defects in the structural dynamics of myoglobin. *EMBO Rep. 2*, 674−679.
(52) Scott, E., Gibson, Q., and Olson, J. (2001) Mapping the pathways for O-2 entry into and exit from myoglobin. *J. Biol. Chem. 276*, 5177−5188.
(53) Srajer, V., Ren, Z., Teng, T., Schmidt, M., Ursby, T., Bourgeois, D., Pradervand, C., Schildkamp, W., Wulff, M., and Moffat, K. (2001) Protein conformational relaxation and ligand migration in myoglobin: A nanosecond to millisecond molecular movie from time-resolved Laue X-ray diffraction. *Biochemistry 40*, 13802−13815.
(54) Ostermann, A., Waschipky, R., Parak, F., and Nienhaus, G. (2000) Ligand binding and conformational motions in myoglobin. *Nature 404*, 205−208.
(55) Schotte, F., Soman, J., Olson, J., Wulff, M., and Anfinrud, P. (2004) Picosecond time-resolved X-ray crystallography: Probing protein function in real time. *J. Struct. Biol. 147*, 235−246.
(56) Nienhaus, K., Deng, P., Olson, J., Warren, J., and Nienhaus, G. (2003) Structural dynamics of myoglobin: Ligand migration and binding in valine 68 mutants. *J. Biol. Chem. 278*, 42532−42544.
(57) Carver, T., Rohlfs, R., Olson, J., Gibson, Q., Blackmore, R., Springer, B., and Sligar, S. (1990) Analysis of the kinetic barriers for ligand-binding to sperm whale myoglobin using site-directed muta-

genesis and laser photolysis techniques. *J. Biol. Chem. 265*, 20007−20020.
(58) Quillin, M., Li, T., Olson, J., Phillips, G., Dou, Y., Ikeda-Saito, M., Regan, R., Carlson, M., Gibson, Q., Li, H., and Elber, R. (1995) Structural and functional effects of apolar mutations of the distal valine in myoglobin. *J. Mol. Biol. 245*, 416−436.
(59) Sugimoto, T., Unno, M., Shiro, Y., Dou, Y., and Ikeda-Saito, M. (1998) Myoglobin mutants giving the largest geminate yield in CO rebinding in the nanosecond time domain. *Biophys. J. 75*, 2188−2194.